Reliable iris localization using integral projection function and 2D-shape properties

Farmanullah Jan*, **Imran Usman, and Shahrukh Agha**

Department of Electrical Engineering, COMSATS Institute of Information Technology,

Park Road, Chak Shahzad, 44000, Islamabad, Pakistan

**Corresponding author: farmanullahs123@yahoo.com*

Received April 20, 2012; accepted May 28, 2012; posted online September 28, 2012

Iris recognition technology recognizes a human based on his/her iris pattern. However, the accuracy of the iris recognition technology depends on accurate iris localization. Localizing a pupil region in the presence of other low-intensity regions, such as hairs, eyebrows, and eyelashes, is a challenging task. This study proposes an iris localization technique that includes a localizing pupillary boundary in a sub-image by using an integral projection function and two-dimensional shape properties (e.g., area, geometry, and circularity). The limbic boundary is localized using gradients and an error distance transform, and the boundary is regularized with active contours. Experimental results obtained from public databases show the superiority of the proposed technique over contemporary methods.

OCIS codes: 150.0150, 100.0100, 110.0110.

doi: 10.3788/COL201210.111501.

Biometric technology recognizes an individual based on his/her physiological and/or physical traits, such as retinas and irises, fingerprints, earprints, signatures, voice, and face, and among others[1]. Among these traits, the face, fingerprints, and voice have long been used for human recognition. However, such traits change as an individual ages and can be artificially duplicated as well[2]. On the other hand, the iris is a unique, stable, and non-invasive biometric. No two individuals have the same iris pattern, including the left and right eyes of the same individual[3]. The iris pattern remains stable over the entire life of a subject, except for some minor changes that occur in the early stages of life after birth[3,4].

A typical iris recognition system includes eye image capture, iris segmentation, feature extraction, and matching[2,3,5]. The term segmentation generally refers to the extraction of features from an image[6,7]. Iris segmentation plays a critical role in the overall recognition accuracy because the accuracy of the other modules also depends on its performance. The iris segmentation module localizes the pupillary (iris inner boundary/pupil circle) and limbic (iris outer boundary/iris circle) boundaries and then detects and excludes any other superimposed noises, such as the eyelids, eyelashes, and/or specular reflections[1−3,5]. Researchers have proposed different methods for iris segmentation, including histogram- and thresholding-based techniques[2,5], gradients and edge detectors[3,4], and genetic algorithms and fuzzy logic[8,9], among others.

The current study focuses on localizing the pupillary and limbic boundaries only (as in Refs. [1, 2, 5]) because iris localization is considered to be the most challenging and time-consuming system module compared with other system modules. Daugman[3] used an integrodifferential operator (IDO) to localize the iris in an eye image. Similarly, Wildes[4] used the gradient edge image and circular Hough transform (CHT) to localize the iris. Given that both the IDO and CHT localize the iris by using a circle approximation, the algorithms that use

these operators generally take longer compared to their counterparts that use the histogram- and thresholding-based techniques[1,2,5,10,11].

Khan *et al.*[2,5] used histogram-, gradients-, and thresholding-based techniques to localize the pupil and iris circles. Khan *et al.*[2] used eccentricity and Ibrahim *et al.*[5] used the standard deviation of the position coordinates of pixels in an object to accurately find the pupil in a binary image. However, after converting the input eye image into a binary level image, the resultant image may contain multiple binary objects (a region of white pixels is called an object) caused by low-intensity regions, such as the eyebrows, eyelashes, hairs, and the pupil region. Therefore, a small round object may have smaller eccentricity and/or standard deviation than the actual pupil object, causing an outage of the system.

Moreover, Khan *et al.*[2,5] were not able to accurately determine the exact center coordinates of the iris circle. Instead, they were only able to determine the y-coordinate and then assumed the x-coordinate of the pupil circle as its x-coordinate. Moreover, they localized the iris by using a circle approximation, which is not circular in reality[12]. These drawbacks may affect the overall system accuracy because a number of iris pixels would be unconsidered or vice versa. Therefore, to resolve such issues, this letter proposes a robust and fast iris localization technique.
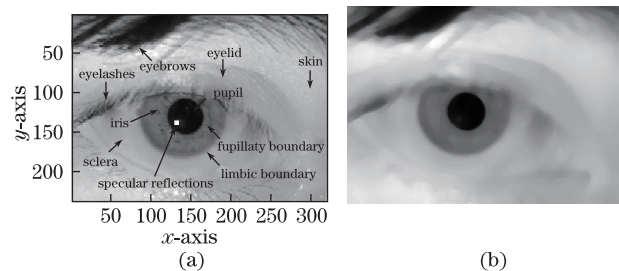

Fig. 1. (a) Input eye image $A(x, y)$ depicting different eye parts; (b) preproccessed eye image $B(x, y)$.

In general, a human eye image [Fig. 1(a)] contains dark (e.g., pupil, eyelashes, eyebrows, and hairs) and bright (e.g., sclera and possibly the skin) regions. The pupil is a low-intensity region, and thus, its localization in the presence of other low-intensity regions is quite challenging. Nevertheless, these low-intensity regions can be differentiated from one another using their geometrical aspects because they have significantly different physical appearances. In addition, the pupil region is relatively more compact than the other low-intensity regions. Following the arguments above, this study proposes a reliable technique that can demarcate the pupillary boundary by using a circle approximation. The proposed technique is comprised of two-dimensional (2D) shape properties (e.g., circularity, area, and geometry) and eye image gray level statistics that can locate the pupil precisely.

Circularity (C) is a measure of compactness of an object, and a circle is the most compact shape. The C of an object can be defined as

$$C = \frac{P^2}{4\pi\tilde{a}},\tag{1}$$

where $\tilde{a}$ and P represent the area and perimeter of an object, respectively. The C of a perfect circle is always one and increases as the shape becomes complicated. The P of a binary image is a set of pixels that belongs to an object and has at least one neighbor that belongs to the background (a region of zeros). The total number of pixels represents the P of an object. However, its precision depends on the methodology used for detecting the boundary pixels, for instance, a four- or an eight-adjacent procedure[13].

The area ($\tilde{a}$) of an object represents the number of pixels in an object calculated as

$$\tilde{a} = \sum_{x=1}^{m_{\mathrm{b}}} \sum_{y=1}^{n_{\mathrm{b}}} I_{\mathrm{b}}(x,y),\tag{2}$$

where m_{b} and n_{b} represent the number of rows and columns of the binary image $I_{\mathrm{b}}(x,y)$ that contains the target object[14].

In this letter, the specular reflections[3] in the input eye image $A(x,y)$ were suppressed prior to the actual iris localization process. The suppression of the specular reflections includes complementing the image $A(x,y)$, filling the holes (a region of zeros surrounded by ones) in the resultant image with a morphological operator '$imfill$'[15], passing the resultant image through a median filter (window size (5×5)) to calm down any boundary artifacts and rapid gray level variations, and finally re-complementing the resultant image to obtain the preprocessed eye image $B(x,y)$. Figure 1(b) shows the preprocessed eye image $B(x,y)$.

The vertical $[f_{\mathrm{v}}(x)]$ and horizontal $[f_{\mathrm{h}}(y)]$ integral projection functions[16], which were used to mark a Seed-location $(x_{\mathrm{s}}, y_{\mathrm{s}})$ in the iris/pupil region in the image $B(x,y)$, can be expressed as

$$f_{\mathrm{v}} = \frac{1}{n} \sum_{i=1}^{n} I(x,y_i), x = 1,2,3,\cdots,m,\tag{3}$$

$$f_{\mathrm{h}} = \frac{1}{m} \sum_{i=1}^{m} I(x_i,y), y = 1,2,3,\cdots,n,\tag{4}$$

where n and m represent the number of columns and rows of $B(x,y)$, respectively. Then, the $(x_{\mathrm{s}}, y_{\mathrm{s}})$-coordinates were extracted as

$$x_{\mathrm{s}} = [x_{\mathrm{b}} \in \{x=1,2,3,\cdots,m\} \text{ such that } f_{\mathrm{v}}(x_{\mathrm{o}}) \text{ is maximum}].\tag{5}$$

$$y_{\mathrm{s}} = [y_{\mathrm{b}} \in \{y=1,2,3,\cdots,m\} \text{ such that } f_{\mathrm{h}}(y_{\mathrm{o}}) \text{ is maximum}].\tag{6}$$

Figure 2(a) shows the $f_{\mathrm{v}}(x)$ and $f_{\mathrm{h}}(y)$ curves along with the seed-location $(x_{\mathrm{s}}, y_{\mathrm{s}})$. Figure 2(b) shows the region of interest (ROI) ROI(x,y), which was centered at $(x_{\mathrm{s}}, y_{\mathrm{s}})$ and each of its side was empirically set to 60% of the width of $B(x,y)$. Hereafter, ROI(x,y) is used as the input image for further processing unless specified otherwise.

Let $(\hat{h})$ represent the histogram (Fig. 3) of ROI(x,y). Generally, the histogram of a human eye image comprises three significant parts, including a lower part that usually represents the low-intensity regions mentioned earlier, a middle part that represents the iris region, and an upper part that represents the bright regions, such as the sclera and the skin. Thus, only the lower half-gray level range ($\gamma = [0 : 127]$) was considered and the upper range was ignored. Next, the γ was bisected into two sub-ranges, γ_{Low} and γ_{High}, as

$$\gamma_{\mathrm{Low}} = (0 \sim \beta),\tag{7}$$

$$\gamma_{\mathrm{High}} = (\beta + 1 \sim 2\beta),\tag{8}$$

where β is the lower gray level saturated limit that represents the bottom 1% of all the gray values in image $B(x,y)$. More details on the calculations can be seen
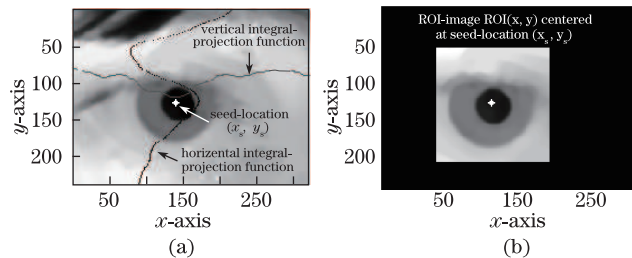

Fig. 2. (a) Preprocessed eye image $B(x,y)$ showing the vertical $f_{\mathrm{v}}(x)$ and the horizontal $f_{\mathrm{h}}(y)$ integral projection functions and the seed-location $(x_{\mathrm{s}}, y_{\mathrm{s}})$. (b) ROI-image ROI$(x,y)$ marked in the image B(x,y); white-dot in the pupil region represents the seed-location $(x_{\mathrm{s}}, y_{\mathrm{s}})$.

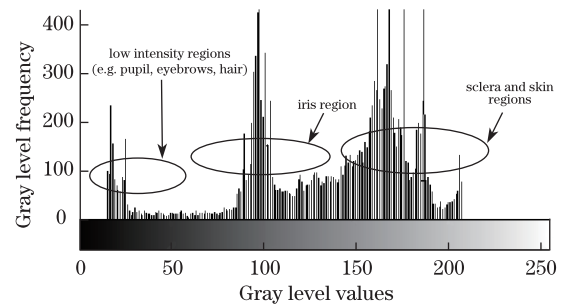

Fig. 3. Histogram $\hat{h}$ of the ROI-image ROI(x,y).

in Ref. [17]. The gray level values (a_1) and (a_2) that correspond to the maximum frequencies in the lower half of $\hat{h}$ were then extracted as

$$a_1 = [\, g_1 \in \gamma_{\text{Low}} \text{ such that } \hat{h}_1(g_1) \text{ is maximum} \,],$$

$$a_2 = [\, g_2 \in \gamma_{\text{High}} \text{ such that } \hat{h}_2(g_2) \text{ is maximum} \,],$$

with $\hat{h}_1 = h(\gamma_{\text{Low}})$ and $\hat{h}_2 = h(\gamma_{\text{High}})$. Then, the following steps were used to localize the circular pupillary boundary in $\text{ROI}(x, y)$:

Step 1 Assign the gray value a_1 to an adaptive threshold (T_{ad}), i.e., $(T_{\text{ad}} = a_1)$.

Step 2 Convert $\text{ROI}(x, y)$ to a binary level image $\text{BW}(x, y)$ as

$$\text{BW}(x,y) = \begin{cases} 1 \text{ if } [(T_{\text{ad}} - \varepsilon) \leqslant \text{ROI}(x,y) \leqslant (T_{\text{ad}} + \varepsilon)] \\ 0 \text{ otherwise} \end{cases}.$$
(9)

In an ideal eye image, the pupil region has uniform gray level intensity, which, however, may not be true under non-ideal conditions because of the non-uniformity of illumination. Therefore, empirically set ε to 6 to compensate for any possible gray level variations in the pupil region. After which, perform a morphological *open*[18] operation on $\text{BW}(x, y)$ by using a structuring element with radius of three. This operation deletes any spurious pixels and isolates the loosely connected binary objects. Next, search any non-zero pixel in $\text{BW}(x, y)$. If no non-zero pixels are found, then assign the gray value a_2 to T_{ad} (i.e., $T_{\text{ad}} = a_2$) and repeat the current step. Otherwise, use a four-adjacent procedure[13] to detect and then invert any gray level values of holes found in $\text{BW}(x, y)$.

As mentioned above, low-intensity regions may cause multiple objects in $\text{BW}(x, y)$. Thus, localizing the pupillary boundary by using the eccentricity (as in Ref. [2]) or standard deviation (as in Ref. [5]) alone may not be feasible unless they are supplemented by other supporting parameters. Such issue was resolved using the 2D-shape properties to localize the pupillary boundary by using a circle approximation $(x_{\text{p}}, y_{\text{p}}, r_{\text{p}})$, where $(x_{\text{p}}, y_{\text{p}})$ and r_{p} are the center and radius of the pupil circle, respectively. Initialize iteration j to one and follow the succeeding steps to select a true pupil object in $\text{BW}(x, y)$.

Step 3 Use the four-adjacent procedure to detect the jth object in $\text{BW}(x, y)$. Compute its area $\tilde{a}(j)$, circularity $C(j)$, and boundary coordinates (X_j, Y_j), and then extract the minima (x_1, y_1) and maxima (x_2, y_2) values of the x- and y-coordinates as

$$(x_1, y_1) = [\min(X), \ \min(Y)], \quad (10)$$
$$(x_2, y_2) = [\max(X), \ \max(Y)]. \quad (11)$$

Calculate the coarse length L and width W as

$$(L, W) = [\max(x_2 - x_1, y_2 - y_1), \min(x_2 - x_1, y_2 - y_1)].$$
(12)

Step 4 If W is less than 60% of L, then the binary object is akin to a strip with a length much greater than its width. This result occurs when the eyebrows, eyeglass frames, or hair-bunches create an object. In this case, increment j by one and repeat Step 3 for the next object. Otherwise, calculate the coarse center (x_j, y_j) and

radius (r_j) as

$$(x_j, y_j) = \left[\frac{(x_1 + x_2)}{2}, \frac{(y_1 + y_2)}{2} \right], \quad (13)$$

$$r_j = \frac{1}{2} \left[\frac{(x_2 - x_1)}{2} + \frac{(y_2 - y_1)}{2} \right]. \quad (14)$$

Then, update the pupil circle vector $(\Re)$ as $\Re = [x_j \ y_j \ r_j]$.

Step 5 Calculate the following conditions:

$$t_0 = [C(j-1) + 0.2] \leqslant C(j) \& C(j) < 1.5,$$
$$t_1 = C(j) \leqslant [C(j-1) - 0.2],$$
$$t_2 = \tilde{a}(j) > \tilde{a}(j-1),$$

Then, perform the following tests:

$$\text{if} \Big[(t_0 == 1 \ \& \ t_2 == 1) | (t_1 == 1 \ \& \ t_2 == 1) \Big] \text{then}$$

$C(j-1) = C(j)$; update the previous value of the circularity.

$\tilde{a}(j-1) = \tilde{a}(j)$; update the previous value of the area.

$\Re(j-1) = \Re(j)$; update the previous value of the pupil circle vector.

else

$\Re(j) = \Re(j-1)$; update the current value of the pupil circle vector by using a previous value.

end

In the pseudo code lines above, $C(j-1)$, $\tilde{a}(j-1)$, and $\Re(j-1)$ hold the previous values of circularity, area, and pupil circle vector, respectively, and the constant-parameter 0.2 in conditions t_0 and t_1 is set empirically. The constant parameter provides an offset in the previous value of circularity, consequently preventing any rapid switching between the previous and current parameters of the binary object. Similarly, the 1.5 in condition t_0 is also set empirically. As stated above, the circularity of a perfect circle is always one and increases as the shape becomes complicated. Therefore, this parameter confines the object circularity range to window (1–1.5).

Increment j by one and repeat the entire process from Step 3 until all the other objects are scanned. However, if no pupil object exists in $\text{BW}(x, y)$ and the current value of T_{ad} is a_1, then repeat the entire process from Step 2 for $T_{\text{ad}} = a_2$. Otherwise, obtain the center and radius parameters of the pupillary boundary as follows: $(x_{\text{p}}, y_{\text{p}}) = [\Re_j(1), \Re_j(2)]$ and $r_{\text{p}} = \Re_j(3)$.

As can be seen in Fig. 2(b), the ROI-image $\text{ROI}(x, y)$ does not include the low-intensity regions, such as the eyebrows, and therefore, the resultant binary image $\text{BW}(x, y)$ would contain only a single binary object that is the pupil object. In this case, the pupillary boundary is extracted without issue of multiple-objects. However, we intentionally converted the entire preprocessed eye image $B(x, y)$ into a binary image $\text{BW}(x, y)$ to show the effectiveness of the proposed technique and defend our claim on the multiple-object issue. The proposed technique successfully detected the actual pupil object in the presence of a fake object caused by the eyebrows (Fig. 4(a)). Figure 4(b) shows the pupillary boundary marked by the pupil circle $(x_{\text{p}}, y_{\text{p}}, r_{\text{p}})$.

Limbic boundary localization poses more difficulties than the pupillary boundary because of the low contrast between the iris and sclera regions and the eyelids and

eyelashes occlusions. Thus, to resolve such issues, this letter proposes an effective limbic boundary localization scheme that includes the following steps:

Step 1 Assume the pupil center (x_p, y_p) as the origin of the image and mark two secure conical sectors, $s_1=$ ($-30°$ to $30°$) and $s_2=$ ($150°$ to $210°$), in the preprocessed eye image $B(x, y)$. These regions are normally free from noises, such as the eyelids and eyelashes. Then, initialize a radial vector (r) and an angular vector (θ) as

$$r = \left\{1.5r_P, \ 1.5r_P + 1, 1.5r_P + 2, \cdots, 3.5r_P\right\}, \quad (15)$$

$$\theta = \left\{0 : \pi/180 : \pi\right\}. \quad (16)$$

Step 2 Use Eq. (17) to extract the one-dimensional (1D) gray level profiles (Ψ_1) along the radial-segments in sector s_1. Assume that the lower and upper ends of each radial segment are located at $1.5r_p$ and $3.5r_p$, with respect to (x_p, y_p), respectively, where r_p is the radius of the pupil circle.

$$\Psi_1(u, t) = B(x(t)\, y(t)), \quad (17)$$

where $x(t) = x_p + r(t)\cos[\theta(u)]$ and $y(t) = y_p + r(t)\sin[\theta(u)]$, with $u = 1, 2, 3, \cdots, \widetilde{m}$ and $t = 1, 2, 3, \cdots, \tilde{n}$. $\widetilde{m}$ represents the number of 1D gray level profiles in sector s_1 and $\tilde{n}$ is the size of vector r, which is the number of points considered along each radial-segment. Use a first-order difference equation[13] to calculate an absolute radial gradient (Δ_1) as

$$\Delta_1(t, u) = |\Psi_1(u, t+1) - \psi_1(u, t)|,$$
$$\text{for } u = 1, 2, \cdots, \widetilde{m} - 1 \text{ and } t = 1, 2, \cdots, \tilde{n} - 1. \quad (18)$$

Step 3 Calculate a distance matrix (D_1) of points with maximum gradient in s_1 around the limbic boundary with respect to (x_p, y_p) as

$$D_1(u) = [r(t_0) \text{ such that } \Delta_1(t, u) \text{ is maximum at } t = t_0]$$
$$\text{For } u = 1, 2, \cdots, \widetilde{m} \text{ and } t = 1, 2, 3, \cdots, \tilde{n}. \quad (19)$$

Step 4 Calculate an error distance transform (χ_1) (Fig. (b)) by taking the absolute difference of each entry with all the other entries in D_1 as

$$\chi_1(i, j) = |D_1(i) - D_1(j)|, i, j = 1, 2, 3, \cdots, n_2. \quad (20)$$

Step 5 Delete the false points in D_1, i.e., a point is deleted if it has 50% of its error-distances (in χ_1) greater than an empirical value of 5, and it is kept as a true point if otherwise (Figs. 5(a) and 5(b)). The resultant array is $\breve{D}_1$. Similarly, calculate a distance matrix $\breve{D}_2$ for the points in sector s_2 and calculate the radius (r_i) for the circular limbic boundary as

$$r_i = 0.5 \left\{ \frac{1}{K_1} \sum_{i=1}^{K_1} \breve{D}_1(i) + \frac{1}{K_2} \sum_{j=1}^{K_2} \breve{D}_2(j) \right\}, \quad (21)$$

where K_1 and K_2 represent the number of the true points in $\breve{D}_1$ and $\breve{D}_2$, respectively. Figure 5(c) shows the limbic boundary marked with a circle approximation (x_i, y_i, r_i). The iris circle has radius r_i and (x_p, y_p) as

its center (x_i, y_i).

Figures 4(c) and 5(c) show the pupillary and limbic boundaries marked with circle approximation, which, in reality, are not circular[12] and require further regularization. Thus, a combination of the radial gradients and Fourier series was used to solve such issue[12]. Firstly, mark two circular bands in the pre-processed eye image $B(x, y)$ such that each band has a width of 11 pixels and is centered at the pupil center (x_p, y_p). The inner and outer bands contain the actual pupillary and limbic boundaries, respectively. Next, localize N points with maximum gradients in each band by using a similar approach as adopted above to localize points around the limbic boundary in sector s_1. N is set to be the perimeter of the concerned circular boundary. For example, $N = 2\pi r_p$ for the pupillary boundary, with r_p as the pupil circle radius.

Let d_1 and d_2 represent the radial distances of the points along the pupillary and limbic boundaries with respect to (x_p, y_p), respectively. d_1 and d_2 were passed through the median filter (3×3 window size) to calm down any rapid variations in the radial distances of the boundary points in each band. The resultant arrays are $\bar{d}_1$ and $\bar{d}_2$. Finally, the resultant arrays were filtered using the Fourier series (active contours, as suggested in Ref. [12]). For demostration purposes, M was set to 25 for the optimal pupillary
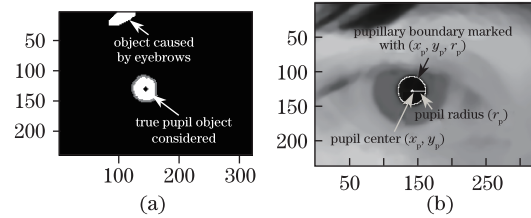

(a)   (b)

Fig. 4. (a) Pupil object marked in image $BW(x, y)$ that shows multiple objects; only two objects in this case. (b) Pupillary boundary marked with the pupil circle (x_p, y_p, r_p) in the preprocessed eye image $B(x, y)$.
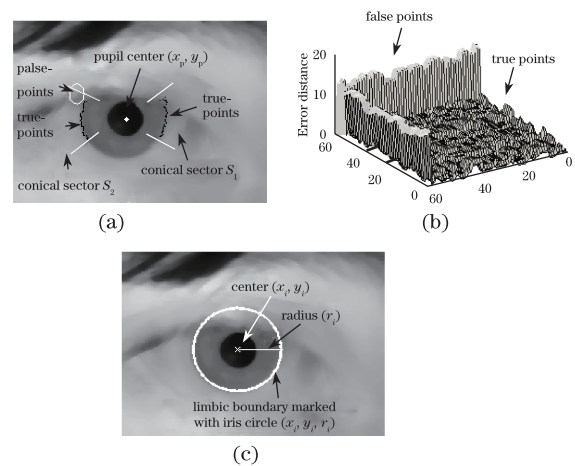

(a)   (b)

(c)

Fig. 5. (a) Preprocessed eye image $B(x, y)$ showing the left and right conical sectors (i.e., S_1 and S_2). Some false-points are shown in the white ellipse in the sector S_2. (b) Error distance transform χ_1. (c) Limbic boundary marked with the iris circle (x_i, y_i, r_i).

boundary. Then, M coefficients for the pupillary boundary were obtained as

$$C_w = \sum_{z=0}^{N-1} d_1(z) \exp(-2\pi \mathrm{i} w z/N), w = 0, 1, 2, \cdots, M-1. \tag{22}$$

The coefficients (C_w, $w = 0, 1, 2, \cdots, M-1$) were then plugged into the following expression to obtain a smooth and close pupillary boundary whose resolution is controlled by M:

$$\widehat{d}_1(s) = \frac{1}{N} \sum_{q=0}^{M-1} C_q \exp(2\pi \mathrm{i} q s/N), s = 0, 1, 2, \cdots, N-1. \tag{23}$$

Similarly, $\widehat{d}_2(s)$ for the limbic boundary was obtained by taking M to be equal to 20 for the optimal boundary fidelity. Figure 6(a) shows the points with maximum gradients along the pupillary and limbic boundaries after the median filtering process. Figure 6(b) shows the pupillary and limbic boundaries filtered using the Fourier series. The proposed technique was tested using Matlab version 7.1 installed on a PC with 2.33 GHz CPU and 1.5 GB RAM. The performance of the proposed technique was evaluated using the public iris databases MMU V1.0[19] and CASIA-Iris-Lamp, which is a subset of CASIA-IrisV3[20]. For accurate results, the accuracy rate (ξ) suggested in Ref. [11] was reused in Ref. [5]. ξ is defined as

$$\xi = \left(\frac{N_1}{N_\mathrm{t}} \times 100\right), \tag{24}$$

where N_1 represents the number of correctly localized irises and N_t is the total number of eye images used in the experiment. Moreover, ξ depends on the accuracy error (φ_err), which is defined as

$$\varphi_\mathrm{err} = \frac{|w_1 - w_2|}{w_1} \times 100, \tag{25}$$

where w_1 and w_2 represent the number of actual and detected iris pixels, respectively. The detected iris pixels are counted using the row-major scanning technique. A localized iris is considered accurate if δ_err is less than 10%, and false if otherwise.

In the first setup, the proposed algorithm was tested on CASIA-Iris-Lamp[20], which contains 16 212 eye images from 411 subjects and has an image resolution of 640×480 (pixel). CASIA-Iris-Lamp offers noise, such as specular reflections, eyebrows, eyelashes, hairs, eyelids, non-uniform illuminations, and off-axis eye images. For better performance, the specular reflections were suppressed at the start of the test. Firstly, 4 080 eye images were used in the experiment. Table 1 shows the accuracy comparison of the proposed technique with some contemporary techniques[3,5,21,22]. Similarly, Fig. 7(a) shows some accurate irises that were localized using the proposed technique.

In the second setup, the proposed technique was tested on the entire MMU V1.0 iris database[19]. MMU V1.0 iris database contains 450 iris images collected from 45 individuals with each image having a resolution of 320×240 (pixel). Iris images from MMU V1.0 iris

Table 1. Comparison with Other Methods for CASIA-IrisV3-Lamp Database (Results Are Taken from the Published Work)

Method	Accuracy (%)
Masek[21]	79.02[a]
Ibrahim et al.[5]	98.28
Koh et al.[22]	99.00
Daugman[3]	96.00[b]
Proposed	99.20

a: results are taken from Ref. [5]; b: results are taken from Ref. [22].

Table 2. Comparison with Other Methods for MMU V1.0 Database (Results Are Taken from the Published Work)

Method	Accuracy(%)
Khan et al.[2]	98.22
Masek[21]	83.92[a]
Dey et al.[11]	98.41[a]
Basit et al.[23]	98.10
Ma et al.[24]	91.02[a]
Proposed	99.25

a: results are taken from Ref. [2].

database contain specular reflections, eyelids, eyelashes, contact lenses, and off-axis eye images. Specular reflections were suppressed prior to the actual iris localization process. Table 2 shows the accuracy comparison results of the proposed algorithm with some contemporary techniques[2,11,21,23,24]. Figure 7(b) shows some irises that have been localized correctly using the proposed technique.

For the temporal analysis, the computational cost of the proposed technique was analyzed using built-in '$profile$'[15] facility of Matlab. In this regard, 1 000 randomly selected eye images were extracted from the two iris databases, and the average time per eye image was estimated. On average, it took 0.2- and 0.8-s time for the MMU V1.0 and CASIA-Iris-Lamp, respectively. Thus, it collectively takes 0.5 sec per eye image for the two iris databases. The proposed technique was evaluated in the Matlab platform, which is a higher-level programming package that runs on general-purpose operating systems[25], such as Windows XP. Its built-in functions contain implicit redundancy. Therefore, any Matlab program usually takes longer compared with other low-level programming languages, such as C/C++. However, if the proposed algorithm is ported onto specialized media, such as Digital signal processors, FPGAs, and CPLDs[26], then it will localize an iris within a fraction of a second.

In conclusion, the key points and achievements of this study are summarized as follows. The proposed technique extracts a sub-image using image integral projection functions to speed up the iris localization process. Then, the proposed technique converts the sub-image to a binary level image by using a bi-valued adaptive threshold based on the histogram and image gray level statistics. The proposed technique utilizes 2D-shape properties to demarcate the pupillary boundary in the
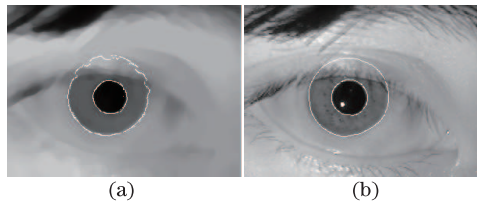
Fig. 6. (a) Preprocessed eye image $B(x, y)$ showing points (having maximum gradients) marked along the pupillary and limbic boundaries after the median filtering process. (b) Original eye image showing the pupillary and limbic boundaries regularized with the Fourier series. Eye image is taken from the MMU V1.0[19].

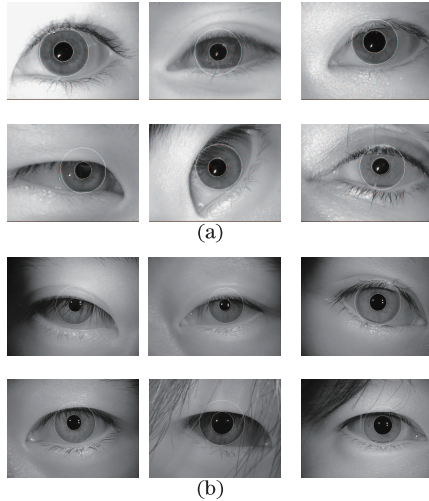Fig. 7. (a) Some randomly selected accurate iris localizations for the CASIA-Iris V3-Lamp[20]. (b) Some randomly selected accurate iris localizations for the MIMU V1[19].

binary image. Notably, the proposed technique localizes the pupil region robustly in the presence of other low-intensity regions, such as eyelashes, eyebrows, and hairs, and it localizes the circular limbic boundary by using a combination of the gradients and error distance transform. Moreover, the proposed technique regularizes the inner and outer boundaries of the iris by using the Fourier series, which compensates for any offset between the pupil and iris centers, as well as the non-circular nature of the iris boundaries. Experimental results show the superiority of the proposed algorithm over contemporary techniques.

References

1. K. W. Bowyer, K. Hollingsworth, and P. J. Flynn, Comput. Vis. Image Und. **110,** 281 (2008).
2. T. M. Khan, M. A. Khan, S. A. Malik, S. A. Khan, T. Bashir, and A. H. Dar, Opt. Lasers Eng. **49,** 177 (2011).
3. J. G. Daugman, IEEE Trans. Pattern Anal Machine Intell. **15,** 1148 (1993).
4. R. P. Wildes, Proc. IEEE **85,** 1348 (1997).
5. M. T. Ibrahim, T. M. Khan, S. A. Khan, M. A. Khan, and L. Guan, Opt. Lasers Eng. **50,** 645 (2012).
6. F. C. Chang and H. M. Hang, IEICE-Trans. Inf. Syst. **E89-D**, 1720 (2006).
7. G. Malathi and V. Shanthi, J. Inf. Hiding Multimedia Signal Process **2,** 332 (2011).
8. P. Puranik, P. Bajaj, A. Abraham, P. Palsodkar, and A. Deshmukh, J. Inf. Hiding Multimedia Signal Process **2,** 227 (2011).
9. T. C. Lin, H. C. Huang, B. Y. Liao, and J. S. Pan, Int. J. Comput. Sci. Eng. Sys. **1,** 253 (2007).
10. A. Basit and M. Y. Javed, Opt. Lasers Eng. **45,** 1107 (2007).
11. S. Dey and D. Samanta, Int. J. Biol. Biomed. Med. Sci. **3,** 180 (2008).
12. J. Daugman, IEEE Trans. Systems, Man, and Cybernetics, Part B: Cybernetics **37,** 1167 (2007).
13. R. C. Gonzalez and R. E.Woods, Digital Image Processing (Prentice Hall, Upper Saddle River, New Jersey 07458).
14. http://www.mathworks.com/help/toolbox/images/ref/regionprops.html (April 18, 2012).
15. Mathworks, http://www.mathworks.com/ (April 18, 2012).
16. Z. H. Zhou and X. Geng, Pattern Recogn. **37,** 1049 (2004).
17. Lower gray level saturated limit, http://www.mathworks.com/help/toolbox/images/ref/stretchlim.html (April 18, 2012).
18. Morphological Open-operation, http://www.mathworks.com/help/toolbox/images/ref/imopen.html (April 18, 2012).
19. MMU iris database, http://pesona.mmu.edu.my/~ccteo/ (April 18, 2012).
20. CASIA iris database, http://www.idealtest.org/findTotalDbByMode.do?mode=Iris (April 18, 2012).
21. L. Masek, "Recognition of Human Iris Patterns for Biometric Identification", B.S. Thesis (University of Western Australia, 2003).
22. J. Koh, V. Govindaraju, and V. Chaudhary, in *Proceedings of 22*th *Int. Conf. Pattern Recognition* (*ICPR*), 2852 (2001).
23. A. Basit, "Iris localization using graylevel texture analysis and recognition using bit planes", PhD. Thesis (National University of Sciences and Technology, Rawalpindi, 2009).
24. L. Ma, T. Tan, Y. Wang, and D. Zhang, Pattern Recogn. **37,** 1287 (2004).
25. General purpose operating systems, http://www.engineersgarage.com/articles/rtos-real-time-operating-system.
26. A. Dasu and S. Panchanathan, in *Proceedings of Int. Conf. Information Technology: Coding and Computing* 300 (2001).